Vibrational and Electronic Properties of Monolayer and Multilayer C_{60} Films on Rh(111)

Abdelkrim Sellidj and Bruce E. Koel*

Department of Chemistry, University of Southern California, Los Angeles, California 90089-0482

*Received: December 2, 1992; In Final Form: June 28, 1993**

We report on investigations of the vibrational and electronic properties of an adsorbed C_{60} monolayer by using high-resolution electron energy loss spectroscopy (HREELS) and electron energy loss spectroscopy (ELS). Spectra were obtained for a C_{60} monolayer and thick multilayers on a Rh(111) single crystal surface. We also investigated the growth mechanism of vapor-deposited C_{60} on Rh(111) and the thermal stability of monolayer and thicker C_{60} films. Bulk films of C_{60} sublime near 500 K, but the C_{60} monolayer is stable up to 750 K, at which point decomposition occurs and graphite-like carbon is formed. Spectra from ultraviolet photoelectron spectroscopy (UPS) and HREELS of a C_{60} monolayer are consistent with molecular adsorption on Rh(111) at or below 300 K. The HREELS spectrum, however, has a much richer structure than that from the surface of a thick layer of C_{60}, which is attributed to a further lowering of the C_{60} symmetry as a result of strong C_{60}–Rh interactions. Electronic transitions in the near-IR to vacuum-UV region from a monolayer of C_{60} on Rh(111) examined by ELS show a new, low-energy excitation at 1.2 eV and considerable broadening of other transitions compared to the case of thick C_{60} films. Adsorption of a monolayer of C_{60} on Rh(111) lowers the work function of the surface by 0.35 eV. This work function change is associated with a positive dipole on the surface implying that C_{60} is a net donor ligand on Rh(111).

1. Introduction

Extensive information now exists on the physical and electronic properties of solid C_{60} from the large number of recent experimental and theoretical studies of this material.[1] Relatively less is known about the properties of thin C_{60} films, and no information is yet available on the properties of monolayer films of C_{60} adsorbed on well-defined, single crystal surfaces on transition metals. The study of ultrathin films of C_{60} on these metal surfaces is of great interest for improving our understanding of the interaction of C_{60} with metal atoms in general.[2-9] In particular, the chemical properties of C_{60} can be strongly affected as a result of the interaction of the transition metal d states with the LUMO of C_{60}. The bonding of C_{60} with metal atoms can be described in terms of interactions of the filled π orbitals with the unfilled d orbitals of the metal and the interaction of the empty π^* (LUMO) orbital with a filled metal d orbital (back-bonding). While π-to-d donation may have little effect on the structure of the valence states of C_{60} because of the localized d–π interaction, electron density that is delocalized from the metal into the π^* orbital by back-bonding reduces the electron affinity of the C_{60} molecule, and the extent of this interaction may strongly influence the chemical properties of C_{60} bonded to the transition-metal atoms.

High-resolution electron energy loss spectroscopy (HREELS) is a powerful probe of vibrational and electronic structure that complements optical spectroscopies and has a very shallow probe depth (of order several atomic layers at surfaces) and often better sensitivity to adsorbed molecular layers. Spectra in the energy range extending from the infrared to the vacuum-UV from HREELS studies of thick C_{60} films have been obtained.[10] Early HREELS spectra were from disordered C_{60} films about 60 Å thick on Si(100).[11,12] More recently, the results of a study of an ordered C_{60} film of about 350-Å thickness on GaSe(0001)[13] have appeared. No such characterization of monolayer C_{60} films has been carried out on metal surfaces.

Other studies on solid C_{60} or on thick C_{60} films using surface science techniques reveal information on C_{60} within the surface layer of these materials.[14] For example, UPS studies of the occupied valence band structure utilizing a He discharge[15] or synchrotron[16] source have been carried out. XPS measurements have provided information on C(1s) core-level binding energies and electronic excitations (through the energies of shake-up satellites).[17,18] Weaver has recently used photoemission and inverse photoemission to probe the electronic structure of C_{60}, C_{70}, and the fullerides.[19] In that paper, and the references therein, the bonding of C_{60} to alkali and alkaline-earth metal atoms in the solid state is discussed. This serves as a useful reference for understanding the bonding of C_{60} to metal surfaces. Of special note are the spectroscopic studies of Ohno et al.[20,21] of C_{60} bonding to several metal and semiconductor surfaces. They observed Fermi level alignment and very little charge transfer. Still, relatively little is known about the details of the bonding interactions that are obviously critical to surface phenomena and the chemical reactivity of adsorbed C_{60}.

In this paper, we report on studies of the vibrational and electronic properties of C_{60} films on Rh(111). Our goals were to determine the nature of C_{60} adsorption on a well-defined, single crystal, reactive metal surface, investigate the vibrational and electronic properties of an adsorbed C_{60} monolayer, and determine the growth mechanism and thermal stability of vapor-deposited C_{60} films on Rh(111).

2. Experimental Apparatus

The experiments were conducted in a three-level ultrahigh-vacuum chamber with a double-pass cylindrical mirror analyzer (CMA) on the top level, low-energy electron diffraction (LEED) optics and a quadrupole mass spectrometer (QMS) for temperature-programmed desorption (TPD) in the middle level, and an LK2000 spectrometer for high-resolution electron energy loss spectroscopy (HREELS) on the bottom level. The base pressure in this chamber was 6×10^{-11} Torr. The Rh(111) crystal was attached to two vertical Ta rods which were fastened to liquid N_2-cooled Cu blocks at the bottom of a differentially pumped *XYZ* manipulator. The sample could be rotated on-axis and translated anywhere between the CMA and the HREELS spectrometer. The sample could be cooled to 88 K or resistively heated to 1500 K.

The Rh(111) sample was cleaned by standard procedures:[22] The sample was sputtered at 5×10^{-5} Torr Ar pressure with a beam voltage of 800 V, annealed to 800 K in 1×10^{-7} Torr of

* Abstract published in *Advance ACS Abstracts*, September 1, 1993.

0022-3654/93/2097-10076$04.00/0

O_2, and repeatedly flashed to 1400 K in vacuum. Sample cleanliness was checked with AES, LEED, and HREELS.

C_{60} material of high purity (>99.9%) was obtained from Prof. C. Reed's group in the Chemistry Department at USC. The C_{60} was purified using a chromatographic method which has been described previously by this group.[23] Thus, we can definitely rule out any significant contributions by C_{70} or other fullerenes in our studies. The C_{60} deposited on the Rh(111) surface was evaporated from a Knudsen cell at a temperature of 600 K. Any toluene solvent that remained in the C_{60} sample was removed by extensive outgassing of the Knudsen cell prior to any deposition. This was checked by looking at the C–H stretching vibration region in HREELS of deposited C_{60} films; no C–H stretching vibrations were detected. The background pressure in the UHV chamber during C_{60} evaporation remained below 1.5×10^{-10} Torr.

The incident beam energy in AES was 3 keV, and the electron beam current was limited to 1.0 μA to reduce as much as possible any damage by the incident electron beam. The spectra were obtained using 1 V peak-to-peak modulation.

The HREELS spectra were recorded in the specular direction with an angle of 60° from the surface normal and a primary electron beam energy of 2.0 eV. The overall energy resolution of the spectrometer was less than 75 cm^{-1} as measured from the fwhm of the elastic peak. Count rates at the elastic peak were about 30–50 kHz. The spectra were normalized to the intensity of the elastic peak.

The electron energy loss spectroscopy (ELS) spectra were also taken with the HREELS spectrometer in the specular geometry with a primary beam energy of either 11 or 30 eV. The incident beam current was $\simeq$6.0 nA, and the energy resolution was 45 meV. Count rates at the elastic peak were 100–150 kHz.

Work function changes were obtained by monitoring the sample-to-ground current versus the sample bias voltage. The electron monochromator, used for HREELS, provided a monoenergetic beam of electrons focused onto the sample, which was oriented perpendicular to the electron beam. The electron beam current to the sample was measured by a picoammeter which had an applied bias voltage referenced to ground. When the bias voltage was sufficiently negative, the current to the sample dropped to zero as the vacuum level of the sample was raised above the energy of the incident electron beam. Changes in the work function are equal to changes in the energy of the vacuum level, and the work function change was determined by measuring the shift in the cutoff voltage obtained from a plot of current versus bias voltage. A decrease in the work function is associated with a lowering of the energy of the vacuum level and a more negative bias voltage.

3. Results and Discussion

3.1. Auger Electron Spectroscopy (AES). In order to characterize the growth mechanism and determine the surface coverage of vapor-deposited C_{60} on Rh(111), we monitored the Rh(302 eV) and C(272 eV) Auger transitions as a function of C_{60} deposition time. This method is commonly used in studies of metal-on-metal depositions[24-26] and should be accurate for determining the monolayer coverage to better than 10% for layer-by-layer or layer-plus-crystallite growth. At low C_{60} coverages the C(272 eV) Auger transition overlaps a weak Rh Auger transition at a slightly smaller energy, and thus monitoring the intensity at 272 eV gives a convolution of increasing C intensity and decreasing Rh intensity. However, using 1-V peak-to-peak modulation, the Rh(302 eV) AES transition has no overlap from the C transition and cleanly provides a monitor of the intensity decrease of the Rh signal due to C_{60} deposition. Here we will discuss only the behavior of the Rh AES signal, noting that the C AES signal is consistent with this behavior.

Figure 1 shows the Rh(302 eV) AES signal as a function of C_{60} deposition time on Rh(111) at 300 K. The uptake curve in

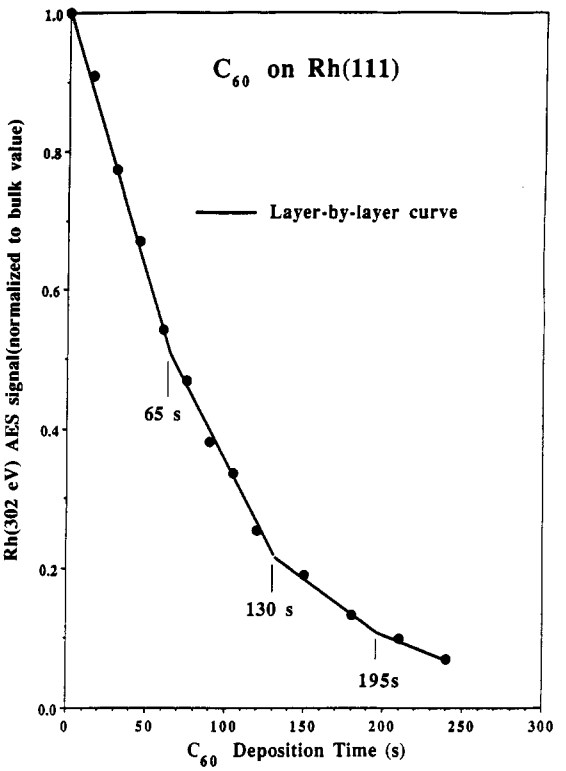

Figure 1. Rh(302 eV) AES signal versus C_{60} deposition time monitoring the vapor deposition of C_{60} on Rh(111) at room temperature.

this figure exhibits three linear segments equally spaced between 0–65, 65–130, and 130–195 s. This behavior is consistent with a layer-by-layer growth mode for C_{60} on Rh(111). The first linear segment corresponds to the growth of the first C_{60} layer, and the "break" or change in slope of the curve at 65 s determines the completion of the first monolayer of C_{60} on Rh(111). This uptake curve was used to estimate the C_{60} coverages during the rest of the experiments. The identification of this coverage as a monolayer is most strongly supported by the annealing experiments described below. However, the assignment of monolayer coverage can be cross-checked qualitatively by a calculation of the electron mean free path for inelastic scattering at 302 eV from the measured attenuation of the Rh signal by a C_{60} monolayer ($\exp(-d/\lambda \cos 42°)$ in our experimental geometry) using d = 8.16 Å, the layer spacing along the (111) axis of the fcc solid. One obtains a value of 16 Å, which is much higher than the expected value of $\simeq$8 Å for other solid materials at this kinetic energy. However, given the hollow nature of the molecule, which partially accounts for the low density of 1.65 g/cm^3 (as compared to 3.51 g/cm^3 for diamond), this value of 16 Å is quite reasonable for C_{60}. Another possible factor is that the density in the C_{60} monolayer could be less than in the close-packed solid due to immobile chemisorption.

The thermal stability of C_{60} films on Rh(111) was also examined by monitoring the Rh(302 eV) AES signal as a function of the annealing temperature. Subsequent to C_{60} deposition at 300 K, the films were annealed to increasing temperatures for 60 s. Figure 2 illustrates the behavior of the Rh(302 eV) AES signal from Rh(111) surfaces containing annealed C_{60} films that were either 1 layer or 15 layers thick. Examining this behavior for a thick C_{60} film first, we see that there is no Rh(302 eV) AES signal detected from 300 to 500 K. At 525 K, the Rh AES signal shows an abrupt increase to the value obtained from a monolayer of C_{60}, a value which was determined from the monolayer break in the AES uptake curve in Figure 1. The sharp increase of the Rh AES signal between 500 and 550 K is attributed to sublimation of solid C_{60}[27] from the Rh surface, leaving a more strongly bonded chemisorbed monolayer of C_{60} on Rh(111). This behavior is the strongest support for identification of monolayer coverage in

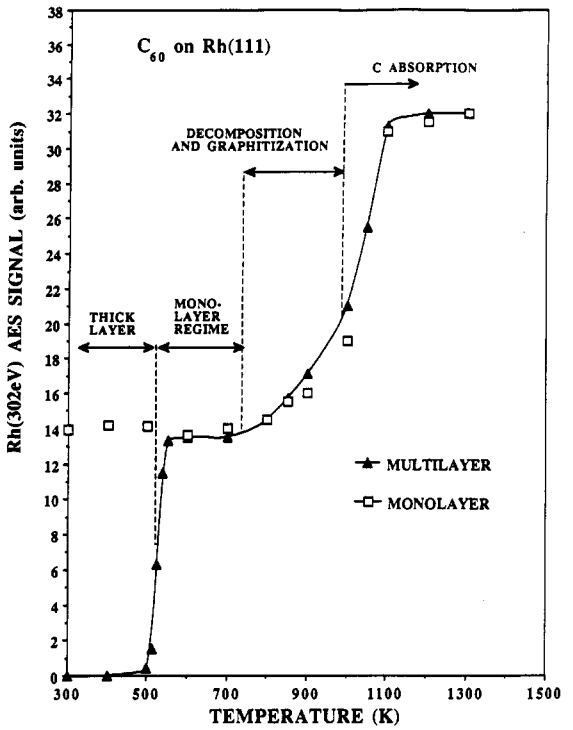

Figure 2. Rh(302 eV) AES signal as a function of annealing temperature for multilayer ($\theta_{C_{60}}$ = 15) and monolayer ($\theta_{C_{60}}$ = 1) C_{60} films on Rh(111).

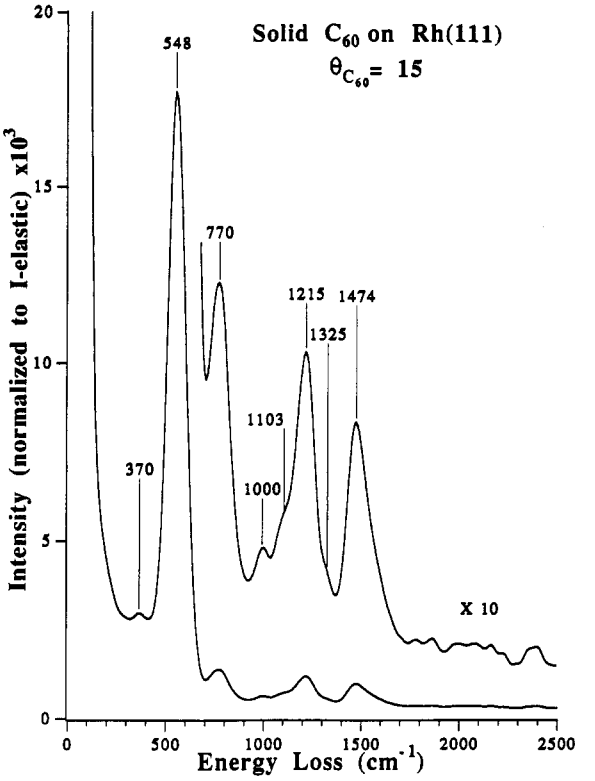

Figure 3. HREELS spectrum from a C_{60} multilayer film ($\theta_{C_{60}}$ = 15) on Rh(111).

Figure 1. From 550 to 750 K the Rh AES signal remains fairly constant, but it starts to increase slowly at higher temperatures. The Rh AES signal continues to increase slowly up to 1000 K, and then it rapidly increases and eventually reaches a value only slightly smaller than the value of the Rh AES signal obtained from the clean Rh(111) surface. The behavior of the Rh AES signal in the 750–1000 K range is attributed to decomposition and graphitization of the C_{60} monolayer. This is based on evidence from HREELS results which will be discussed in the following section. The sharp increase of the Rh AES signal above 1000 K is attributed to decomposition of the graphite-like carbon and carbon diffusion into the bulk of the Rh sample.

Figure 2 also shows the behavior of the Rh AES signal from a monolayer of C_{60} as a function of annealing temperature. The Rh(302 eV) AES signal is fairly constant in the 300–750 K temperature range, and then this monolayer curve follows the same curve as the signal obtained from a thick C_{60} film.

In summary, these studies demonstrate that vapor-deposited C_{60} on Rh(111) at 300 K grows initially in a layer-by-layer mode. In addition, a monolayer of C_{60} on Rh(111) is stable up to 750 K, which is attributed to a relatively strong chemisorption bonding interaction between the Rh surface and C_{60} molecules.

3.2. Ultraviolet Photoelectron Spectroscopy (UPS). He (I)-UPS spectra obtained with a high-pressure discharge lamp for a thick C_{60} multilayer on Rh(111) at 300 K showed excellent agreement with previously published UPS spectra of C_{60} films.[15] The valence band spectrum of C_{60} within 10 eV of the Fermi level (E_F) shows a very distinct five-band structure that characterizes the electronic structure of the C_{60} molecule. UPS spectra that we obtained for the C_{60} monolayer on Rh(111) at 300 K were nearly identical to the multilayer spectra. All of the valence band peaks were seen with the same positions, widths, and relative intensities, except for a shift of 0.13 eV toward E_F of both of the highest-lying valence bands due to the π-derived orbitals. (Peaks from these orbitals occur at 3.30 and 1.95-eV binding energy for the C_{60} multilayer.) Apart from a very small and structureless emission from the Rh valence band near E_F, which is not completely attenuated by the C_{60} monolayer formed in this case, no evidence is seen for any features that could be attributed to new Rh–C_{60} bonding derived orbitals. These results enable us to make two valuable conclusions. First, the chemisorbed monolayer of C_{60} on Rh(111) at 300 K is molecular, as determined by UPS. Second, the bonding interactions of C_{60} with Rh(111) results in very little net charge transfer (much less than one electron) to the adsorbed C_{60} molecule, as judged by the absence of any LUMO-derived band with appreciable intensity.

3.3. High-Resolution Electron Energy Loss Spectroscopy (HREELS). A HREELS spectrum taken from a thick film of C_{60} at 300 K is shown in Figure 3. Eight distinct losses can be identified. The most intense loss was recorded at 548 cm^{-1}, and relatively less intense losses were recorded at 770, 1215, and 1474 cm^{-1}. The 370, 1000, 1103, and 1325 cm^{-1} loss peaks are rather weak. In Table I we list our results along with a previous HREELS study of a thick film of C_{60}[11,12] and the energies of some vibrational modes of bulk C_{60} identified by IR[28] and Raman.[6] There are 174 vibrational modes of C_{60}, but there are only 46 distinct modes because many of them are degenerate. Four of the modes are IR-active and 10 modes are Raman-active.[29]

The loss peaks at 548, 1215, and 1474 cm^{-1} in the HREELS spectrum in Figure 3 are associated with normal modes of C_{60} that are dipole active. This identification is based on off-specular HREELS experiments,[16] wherein the intensities of the loss peaks at 548, 1215, and 1474 cm^{-1} drop dramatically in the off-specular spectra, clearly indicating that these losses stem from vibrational modes of C_{60} that are dipole-active. Several other modes that are also observed can be accounted for by either negative ion resonance or impact scattering mechanisms. Alternatively, we do not rule out the fact that the weaker losses in the specular HREELS spectrum could be weakly dipole active due to a reduction in the symmetry of the C_{60} molecules *at the surface* in the solid phase. HREELS, being a much more surface sensitive spectroscopy than IR, is more sensitive to these changes if they occur. We are currently investigating further details of the electron scattering mechanisms on multilayer and monolayer C_{60} films on Rh(111).[30]

Several small differences exist between our thick film results and those from a HREELS study of a 60 Å thick C_{60} film on Si(100),[11,12] as listed in Table I. The most intense loss peaks in

TABLE I: Vibrational Frequencies (cm^{-1}) of C_{60} Films

		HREELS		
IR[a] (ref 28)	Raman[a] (ref 6)	multilayer (refs, 11, 12)	multilayer on Rh(111) (this work)	monolayer on Rh(111) (this work)
	272	274		
		355	370	370
				400
	432	444		
	485			
	495			
527				
	534	532	548	533
	566			
576				
	710	686		
	772	758	770	770
		968		955
			1000	1000
	1100	1097	1103	1090
				1135
1182				
			1215	1215
	1249	1258		1252
			1325	1348
1429	1425			1422
		1452		
	1468		1474	1481
	1574	1565		1585

[a] Crystalline solid C_{60}.

their spectra were recorded at 532, 758, 1258, and 1565 cm^{-1}. This is different from our spectra where the most intense losses were recorded at 548, 770, 1215, and 1474 cm^{-1}. Also, the dipole-active modes identified in our HREELS spectrum from a thick C_{60} layer at 548, 1215, and 1474 cm^{-1} do not exactly match with the four intense IR bands at 527, 576, 1182, and 1429 cm^{-1}.[28] These differences are attributed to dipole–dipole coupling between the C_{60} molecules near the C_{60} surface. The loss peak at 548 cm^{-1} cannot be attributed to convolution of the corresponding IR bands at 526 and 577 cm^{-1}, since the fwhm of the loss peak at 549 cm^{-1} and that of the elastic peak were practically the same, and thus this feature can be attributed to a single vibrational mode of C_{60}. The 548, 1215, and 1474 cm^{-1} loss energies can be assigned to the same modes responsible for IR absorption at 526, 1183, and 1429 cm^{-1} with blue shifts of 22, 33, and 35 cm^{-1}, respectively, mostly due to long-range dipole–dipole coupling in the C_{60} layer near the surface. We cannot rule out that these shifts might be due to symmetry reduction in the C_{60} molecules in the vicinity of the surface of the thick C_{60} film. Disorder effects in the thick films are important, and HREELS studies[10,13] on disordered, thick C_{60} films on Si(100) and well-ordered, epitaxial thick C_{60} films on GaSe(0001) show differences in the spectra. The HREELS spectra in the latter case detected all four IR-active modes of C_{60}.

Figure 4 displays a HREELS spectrum from a monolayer of C_{60} on Rh(111) at 300 K. The vibrational losses identified from this spectrum are listed in Table I. In this case, 14 vibrational losses were recorded, with the most intense features at 533, 770, 1215, 1252, 1481, and 1585 cm^{-1}. Relatively weaker losses can be seen at 370, 400, 955, 1000, 1090, 1135, 1348, and 1422 cm^{-1}. It is difficult at this point to know which modes are responsible for the observed vibrational spectrum. However, the similarity of the spectrum to that from the multilayer is consistent with molecular adsorption in the chemisorbed monolayer. The increased number of losses in the monolayer HREELS spectrum in comparison to the multilayer spectrum is attributed to a further reduction in the symmetry of the C_{60} molecules as a result of the interaction with the surface Rh atoms. In addition, molecular vibrations parallel to the surface can generate modulations in the charge associated with the C_{60}–Rh bond, inducing a dynamic

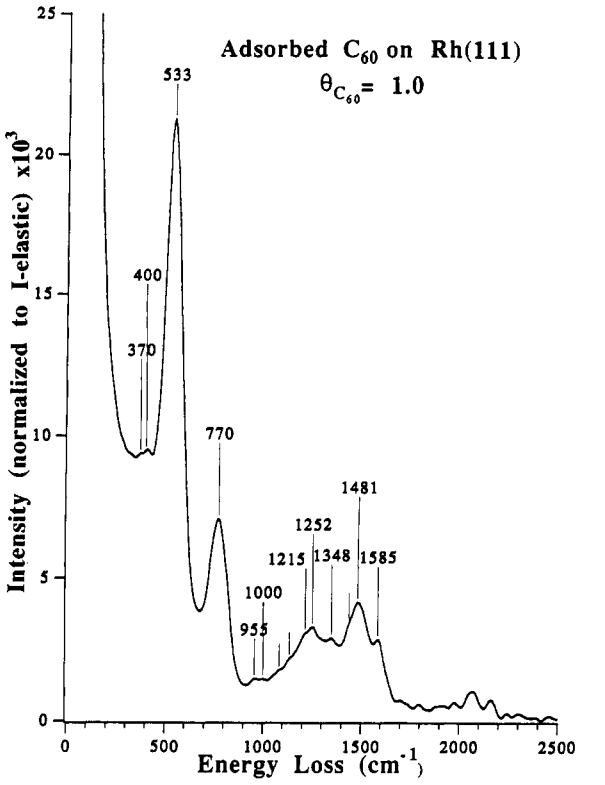

Figure 4. HREELS spectrum from a monolayer C_{60} film on Rh(111).

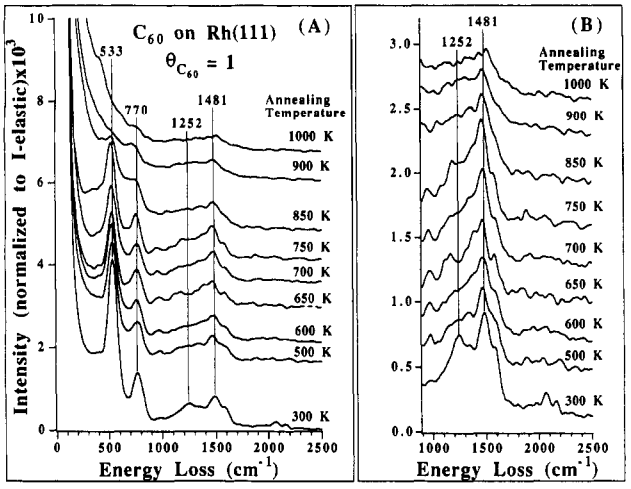

Figure 5. HREELS spectra from a monolayer C_{60} film on Rh(111) annealed to increasing temperatures.

dipole perpendicular to surface, and hence non-dipole-active modes can be observed in HREELS experiments.

Figure 5 shows HREELS spectra from a monolayer of C_{60} Rh(111) annealed to various temperatures. Over the 300–750 K range, the HREELS spectra show several changes, but the spectra retain the characteristic features of the monolayer, namely, peaks near 370, 533, 770, 955, 1252, 1481, and 1585 cm^{-1}. The 533 cm^{-1} loss shifts to 520 cm^{-1}. Its intensity drops slightly upon annealing to 500 K and then remains constant up to 750 K. The intensity of the 1252 cm^{-1} loss peak decreases after annealing above 500 K, and the 1481 cm^{-1} loss peak shifts to 1470 cm^{-1}. Changes in the structure of the spectra in the 900–1250 cm^{-1} range are also clearly visible. These changes in the HREELS spectrum of a monolayer of C_{60} could possibly be due to changes in the bonding configuration of C_{60} molecules to the Rh atoms, with no evidence of any large change in the chemical nature of the C_{60} molecules.

Large changes in the C_{60} monolayer HREELS spectrum occur after annealing to 850 K. These changes are not simply due to

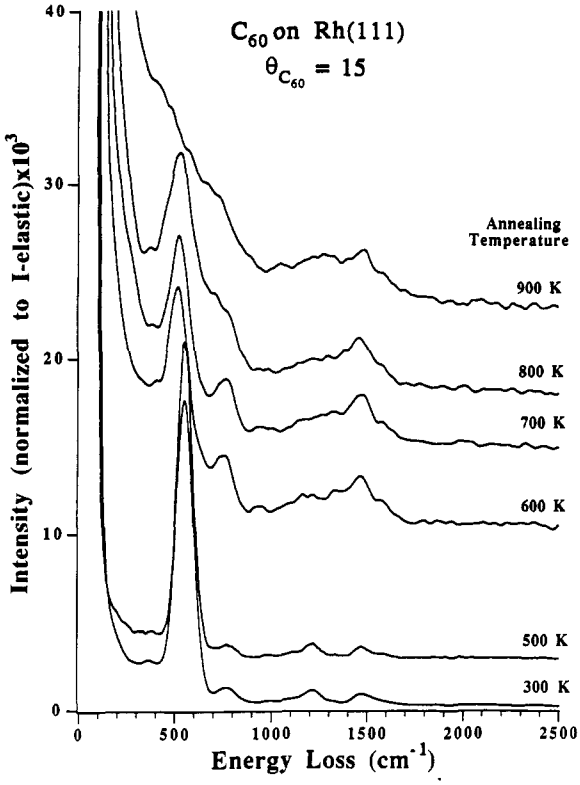

Figure 6. HREELS spectra from a C_{60} multilayer film ($\theta_{C_{60}}$ = 15) on Rh(111) annealed to increasing temperatures.

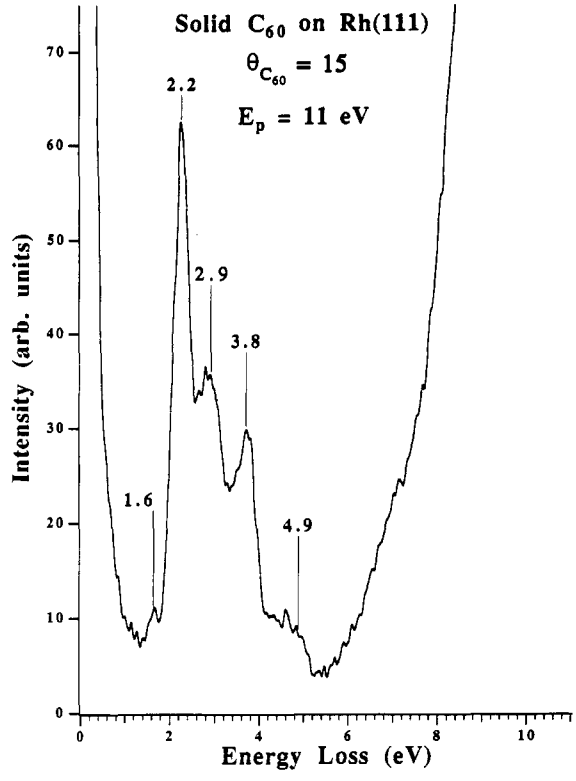

Figure 7. ELS spectrum at E_p = 11eV from a C_{60} multilayer film ($\theta_{C_{60}}$ = 15) on Rh(111).

C_{60} desorption since the AES curves in Figure 2 do not show a large change in the Rh signal in this small temperature interval. At 900 K the spectrum consists of two broad peaks at 750 and 1480 cm^{-1} and a broad structure extending from 1000 to 1400 cm^{-1}. In general, the HREELS spectra from the annealed C_{60} monolayer retained most of the loss structure of C_{60} in the 1000–1600 cm^{-1} range. This may result from the large C_n fragments formed on the surface from C_{60} decomposition. At the highest temperatures, small domains of graphite may be formed in addition to carbon dissolution into the bulk of the Rh crystal. The calculated phonon density of states of graphite shows maxima at 466, 775, 1340, 1420, and 1610 cm^{-1}.[31] Since most of the loss structure in the HREELS spectra of annealed C_{60} films falls within this range, C_{60} graphitization may begin to take place when a C_{60} monolayer on Rh(111) is annealed above 750 K.[32]

Figure 6 shows HREELS spectra from a thick C_{60} film annealed to various temperatures. In this case, the spectra exhibit no apparent changes in the loss structure when the film is annealed in the 300–500 K temperature range. Above 500 K, the HREELS spectra display features similar to those seen for the annealed C_{60} monolayer. This is consistent with the AES study of the thermal stability of C_{60} films described in the preceding section.

3.4. Electron Energy Loss Spectroscopy (ELS). Turning now to electronic excitation energies, Figures 7 and 8 show ELS spectra taken in the specular geometry with a primary beam energy, E_p, of 11 and 30 eV, respectively, from a thick multilayer of C_{60}. For E_p = 11 eV, the lowest energy loss peak is recorded at 1.6 eV. A sharp and intense peak is observed at 2.2 eV, relatively intense peaks can be distinguished at 2.9 and 3.8 eV, and a weak feature is seen near 4.9 eV. In the spectrum using E_p = 30 eV, the same low-energy transitions are recorded, but more transitions are observed above 4 eV. Two peaks are outstanding at 4.9 and 6.6 eV. The latter shows a broad shoulder at 6.1 eV. Finally, a weaker and broader feature is clearly visible at 7.8 eV. These results are consistent with previous ELS studies of thick C_{60} films on Si(100) conducted by Lucas et al.[12]

The calculated HOMO–LUMO energy separation for C_{60} is 1.65–1.85 eV.[33-38] The corresponding electronic transition is not

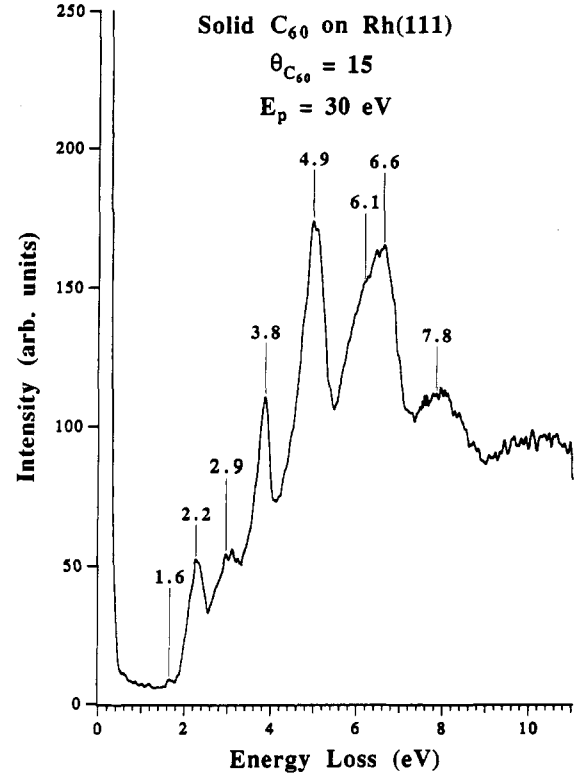

Figure 8. ELS spectrum at E_p = 30 eV from a C_{60} multilayer film ($\theta_{C_{60}}$ = 15) on Rh(111).

dipole active, but because of the symmetry alteration of C_{60} in the solid phase, this transition could be weakly allowed. This is probably the origin of the 1.6-eV peak. The energy separation between the second highest-lying occupied orbital and the LUMO was calculated at 2.7 eV, and the corresponding electronic transition is dipole-allowed. The sharp peak at 2.2 eV can be attributed to this transition. Interpretation of these data must take into account band structure effects due long-range order

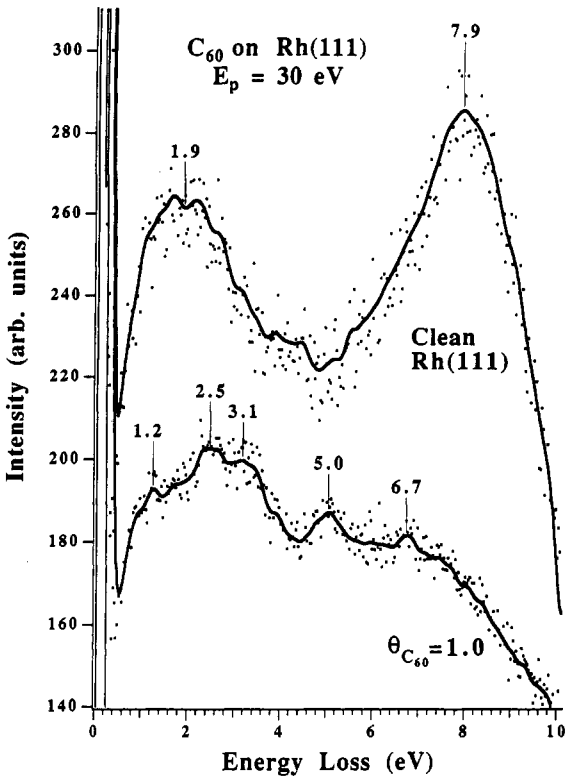

Figure 9. ELS spectra at E_p = 30 eV from a clean Rh(111) surface and a C_{60} monolayer on Rh(111). A solid curve obtained by smoothing the measured data is shown in addition to the measured data points in order to discern the spectral features.

that might be present in these films. First principle calculations by Ching et al.,[39] using the self-consistent, orthogonalized linear combination of atomic orbitals (OLCAO) method, show a rich band structure for an fcc crystal of C_{60}. Their calculations characterize the valence band (VB) and conductance band (CB) as having five major features each (labeled V1–V5 and C1–C5, respectively) with bandwidths ranging from 0.5 to 1.0 eV. We assign the 2.9-eV peak to an interband transition between the HOMO-derived VB and the second lowest CB originating from the next LUMO of isolated C_{60} molecules (transition labeled V2 → C1 in ref 39). The loss peaks at 3.8, 4.9, and 6.1 eV are assigned to electronic transitions as described in ref 39: 3.8 eV, V1 → C3 and V2 → C2; 4.9 eV, V2 → C3 and V1 → C4; 6.1 eV, V1 → C5 and V2 → C4. The peak at 6.6 eV is attributed to collective excitations of the π electrons. This feature was also predicted by the calculations of Ching et al.[39] The broad feature centered around 7.8 eV is attributed to the first ionization potential of C_{60}.

ELS spectra from clean Rh(111) and a monolayer of C_{60} adsorbed on Rh(111) are displayed in Figure 9. The clean Rh(111) surface yields two broad features at about 1.9 and 7.9 eV. The first peak corresponds to interband transitions from the occupied d bands to empty bands near the Fermi level, while the second feature is associated with a bulk or surface plasmon of Rh(111). Adsorption of a C_{60} monolayer attenuates these peaks and causes many new peaks to appear that are closely related to the solid C_{60} peaks. Peaks at 1.2, 2.5, 3.1, 5.0, and 6.7 eV can be seen in the ELS spectrum from a monolayer of C_{60} shown in Figure 9. These peaks are extremely weak and much broader in comparison to those ELS peaks observed on a multilayer of C_{60} (see Figures 7 and 8). This is due to heavy screening (by the metal electrons) of the electric dipoles associated with the electronic transitions induced in the C_{60} molecules adsorbed on the Rh(111) surface.

The electronic structure of the valence band of C_{60} can be considerably altered as a result of the interaction of C_{60} with metal atoms, with one of the major effects being the occupation of the π^* orbital (t_{1u}) of C_{60}. Any partial occupation of the π^* LUMO orbital (t_{1u}) of the C_{60} molecules in the monolayer will induce a new transition, $t_{1u} \rightarrow t_{1g}$, which is dipole-allowed. The $t_{1u} \rightarrow t_{1g}$ transition for C_{60}^- was calculated at 1.1 eV[40-42] and measured at 1.15 eV.[43-47] We therefore assign the peak at 1.2 eV to electronic transitions between the newly occupied band derived from the t_{1u} orbital of C_{60} and the band derived from the t_{1g} orbital. The features at 2.5, 3.1, and 5.0 eV are attributed to $\pi \rightarrow \pi^*$ transitions, but a rigorous assignment of these features to specific π–π^* interband transitions will require a full band structure calculation on a C_{60} monolayer on Rh(111), in which the Rh–C_{60} interaction is adequately taken into account. Finally, the loss peak at 6.7 eV is attributed to collective excitation of a π plasmon analogously to the 6.6-eV peak seen from the thick C_{60} layer.

3.4. Work Function Measurements. The work function of Rh(111) is 5.4 eV.[48] Submonolayer coverages of C_{60} on Rh(111) decrease the work function, and adsorption of a monolayer of C_{60} on Rh(111) decreases the work function by $\cong$0.35 eV. Work function changes are commonly interpreted as directly proportional to the effective dipole moment induced by adsorbates on the surface. If n is the adsorbate density, μ the induced dipole moment, and α the polarizability of the adsorbate, then the work function change ($\Delta\phi$) is given by[49]

$$\Delta\phi = -en\mu/\epsilon_0[1 + (9/4\pi)\alpha n^{3/2}] \quad (1)$$

where ϵ_0 is the vacuuum permittivity. A value for the size of the effective dipole can be calculated from work function changes. Assuming that the C_{60} monolayer on Rh(111) has an fcc(111) structure with a lattice constant of 14.17 Å,[50] the surface density of C_{60} is then $n = 1.0 \times 10^{14}$ molecules/cm^2. With a value of 65.5×10^{-24} cm^3 for the polarizability, α, obtained from an ab initio calculation,[21] and the measured work function change of –0.35 eV, a value of $\mu = +2.7 \times 10^{-30}$ C m is obtained. This can be compared to $\mu = +6.7 \times 10^{-30}$ C m for benzene, C_6H_6, on Rh(111).[51] However, this comparison is only approximate, since the polarizability of *adsorbed* C_{60} is unknown (and it is probably much larger than the gas-phase value). The nature of the C_{60} interaction with Rh(111) may be similar to that of benzene with Rh(111), and this can be described in terms of π–d bonding with delocalization of charge from C_{60} to the metal and d–π^* back-bonding with delocalization of charge in the opposite direction. The strength of this interaction controls the extent of the delocalization, possible rehybridization of the carbon atoms involved, and whether or not charge transfer occurs. The direction of the effective surface dipole and the sign of the work function change are determined by the total charge transfer between the C_{60} and the Rh surface. For C_{60} on Rh(111) the decrease in the work function upon adsorption indicates that π-to-d donation is larger than the d-to-π^* back-donation, or in other words, the charge state of chemisorbed C_{60} is dominated by the π-donor interaction with the d states of the Rh atoms. Moreover, since the size of the effective dipole associated with the C_{60}–Rh complex is smaller than that of benzene, the compensation effects from d–π^* back-bonding seem to be larger for C_{60}. Back-bonding in C_{60} is enhanced because of the relatively low energy of the LUMO of C_{60}.

Several organometallic compounds involving the C_{60} ligand and Pt[6] show an η_2 coordination. This could be the coordination geometry of C_{60} adsorbed on Rh(111). However, the accessibility of many Rh atoms on the Rh(111) surface would easily allow for bonding through the five or six-member rings that form the faces of C_{60}, and this could lead to a stronger chemisorption bond. Obviously, the details of the geometry and the nature of the chemisorption bond of C_{60} on transition metals are crucial issues that remain to be resolved.

4. Conclusions

AES indicates that vapor-deposited C_{60} grows in a layer-by-layer mode for at least three layers on Rh(111) at room temperature. HREELS and ELS have been used to characterize the vibrational and electronic properties of a monolayer of C_{60} adsorbed on Rh(111), and these are compared to those of the surface layers of solid C_{60} (thick multilayers). The HREELS spectrum from a monolayer of C_{60} on Rh(111) shows several losses which do not appear in the HREELS spectra of multilayers of C_{60}. The appearance of these features is attributed to a further reduction in the symmetry of C_{60} molecules as a result of strong interactions with the Rh surface. Thermal desorption of C_{60} from multilayer films commences near 500 K, leaving a C_{60} monolayer on the surface, and thus 500 K is the upper limit of stability of thick films. HREELS and UPS indicates molecular chemisorption of C_{60} on Rh(111) at or below 300 K. Annealing experiments do not indicate any large changes in the chemical nature of the C_{60} monolayer up to 750 K, but the bonding configuration of C_{60} to the Rh(111) surface may change. Decomposition occurs at 750 K and graphite-like carbon is formed. Adsorption of a monolayer of C_{60} on Rh(111) lowers the work function of the surface by 0.35 eV, and this change is associated with a positive dipole on the surface. This agrees with UPS spectra of chemisorbed C_{60} on Rh(111) that show the absence of a new LUMO-derived band (which is present for K_3C_{60} and K_6C_{60}). Thus, the formation of the chemisorption bond of C_{60} on Rh(111) is such that C_{60} is a net donor ligand. Electronic transitions in the near-IR to vacuum-UV region from a monolayer of C_{60} on Rh(111) examined by ELS show a new, low-energy excitation near 1.2 eV and considerable broadening of other transitions compared to thick C_{60} films. The spectra of C_{60} multilayers can be assigned using existing band structure calculations. The spectra of the C_{60} monolayer show the effects of changes in the electronic structure of C_{60} due to chemisorption, and the low-energy excitations are interpreted in terms of transitions between new electronic states formed by Rh–C_{60} interactions.

Acknowledgment. We gratefully acknowledge useful discussions with Dr. Deborah H. Parker and Prof. Christopher A. Reed. We thank Prof. Reed for providing the C_{60} sample and Dr. J. J. Pireaux for providing several papers to us prior to their publication. Also, we thank Mike Voss for his help in taking and analyzing some of the AES data. This work was partially supported by the U.S. Department of Energy, Office of Basic Energy Sciences, Chemical Sciences Division.

References and Notes

(1) Kroto, H. W.; Allaf, A. W.; Balm, S. P. *Chem. Rev.* **1991**, *91*, 1213.
(2) Garrell, R. L.; Herne, T. M.; Szafranski, C. A.; Diederich, F.; Ettl, F.; Whetten, R. L. *J. Am. Chem. Soc.* **1991**, *113*, 6302.
(3) Zhang, Y.; Gao, X.; Weaver, M. J. *J. Phys. Chem.* **1992**, *96*, 510.
(4) Burstein, E.; Erwin, S. C.; Jiang, M. Y.; Messmer, R. P. *Phys. Scr.* **1992**, *T42*, 207.
(5) Akers, K. L.; Cousins, L. M.; Moskovits, M. *Chem. Phys. Lett.* **1992**, *190*, 614.
(6) Chase, B.; Fagan, P. L. *J. Am. Chem. Soc.* **1992**, *114*, 2252.
(7) Kelly, M. K.; Etchegoin, P.; Fuchs, D.; Krätschmer, W.; Fostiropoulos, K. *Phys. Rev. B* **1992**, *46*, 4963.
(8) Fagan, P. J.; Calabrese, J. C.; Malone, B. *Acc. Chem. Res.* **1992**, *25*, 134.
(9) Fann, Y. C.; Singh, D.; Jansen, S. A. *J. Phys. Chem.* **1992**, *96*, 5817.
(10) Lucas, A. A. *J. Phys. Chem. Solids* **1992**, *53*, 1415.
(11) Gensterblum, G.; Pireaux, J. J.; Thiry, P. A.; Caudano, R.; Vigneron, J. P.; Lambin, Ph.; Lucas, A. A.; Krätschmer, W. *Phys. Rev. Lett.* **1991**, *67*, 2171.
(12) Lucas, A. A.; Gensterblum, G.; Pireaux, J. J.; Thiry, P. A.; Caudano, R.; Vigneron, J. P.; Lambin, Ph.; Krätschmer, W. *Phys. Rev. B* **1992**, *45*, 13694.
(13) Gensterblum, G.; Li-Ming, Y.; Pireaux, J. J.; Thiry, P. A.; Caudano, R.; Lambin, Ph.; Lucas, A. A.; Krätschmer, W.; Fischer, J. E. *J. Phys. Chem. Solids* **1992**, *53*, 1427.
(14) Wertheim, G. K.; Buchanan, D. N. E.; Chaban, E. E.; Rowe, J. E. *Solid State Commun.* **1992**, *83*, 785.
(15) Lichtenberger, D. L.; Nebesny, K. W.; Ray, Ch. D.; Huffman, D. R.; Lamb, L. D. *Chem. Phys. Lett.* **1991**, *176*, 203.
(16) Vertel, I. V.; et al. *Phys. Rev. Lett.* **1992**, *68*, 784.
(17) Weaver, J. H.; et al. *Phys. Rev. Lett.* **1991**, *66*, 1741.
(18) Benning, P. J.; et al. *Phys. Rev.* **1991**, *B44*, 1962.
(19) Weaver, J. H. *J. Phys. Chem. Solids* **1992**, *53*, 1433.
(20) Ohno, T. R.; Chen, Y.; Harvey, S. E.; Kroll, G. H.; Weaver, J. H.; Haufler, R. E.; Smalley, R. E. *Phys. Rev.* **1991**, *B44*, 13747.
(21) Ohno, T. R.; Chen, Y.; Harvey, S. E.; Kroll, G. H.; Benning, P. J.; Weaver, J. H.; Chibante, L. P. F.; Smalley, R. E. *Phys. Rev.* **1993**, *B47*, 2389.
(22) Musket, R. G.; McLean, W.; Colmenares, C. A.; Makowiecki, D. M.; Siekhaus, W. J. *Appl. Surf. Sci.* **1982**, *10*, 143.
(23) Bhyrappa, P.; Penicaud, A.; Kawamoto, M.; Reed, C. A. *J. Chem. Soc., Chem. Commun.* **1992**, *13*, 936.
(24) Sellidj, A.; Koel, B. E. *Surf. Sci.* **1993**, *281*, 223.
(25) Koel, B. E.; Sellidj, A.; Paffett, M. T. *Phys. Rev. B* **1992**, *46*, 7846.
(26) Heitzinger, J. M.; Gebhard, S. C.; Parker, D. H.; Koel, B. E. *Surf. Sci.* **1992**, *260*, 151.
(27) Tokmakoff, A.; Haynes, D. R.; George, S. M. *Chem. Phys. Lett.* **1991**, *186*, 450.
(28) Hare, J. P.; Dennis, T. J.; Kroto, H. W.; Taylor, R.; Allaf, A. W.; Balm, S.; Walton, D. R. M. *J. Chem. Soc., Chem. Commun.* **1991**, 412.
(29) Weeks, D. E.; Harter, W. G. *J. Chem. Phys.* **1989**, *90*, 4744.
(30) Sellidj, A.; Koel, B. E. *Chem. Phys. Lett*, to be submitted.
(31) Nicklow, R.; Wakabayashi, N.; Smith, H. G. *Phys. Rev. B* **1972**, *5*, 4951.
(32) Graphite modes that are normally not dipole active can become active as a result of symmetry reduction either from graphitic-like carbon (but not graphite sheets) or graphitic carbon due to interaction with the Rh surface. Alternatively, we cannot rule out the coadescence of C_{60} molecules into larger fullerines (Yeretzian, C.; Hansen, K.; Dieterich, F.; and Whetten, R. L. *Nature* **1992**, *359*, 44).
(33) Ozaki, M.; Takahashi, A. *Chem. Phys. Lett.* **1986**, *127*, 242.
(34) Rosén, A.; Wästberg, B. *J. Chem. Phys.* **1989**, *90*, 2525.
(35) Fowler, P. W.; Lazzeretti, P.; Zanasi, R. *Chem. Phys. Lett.* **1990**, *165*, 79.
(36) Dunlap, B. I.; Brenner, D. W.; Mintmire, J. W.; Mowrey, R. C.; White, C. T. *J. Phys. Chem.* **1991**, *95*, 5763.
(37) Saito, S.; Oshiyama, A. *Phys. Rev. Lett.* **1991**, *66*, 2637.
(38) Kobayashi, K.; Kurita, N.; Kumahora, H.; Tago, K.; Ozawa, K. *Phys. Rev. B.* **1992**, *45*, 13690.
(39) Ching, W. Y.; Huang, M. Z.; Xu, Y. N.; Harter, W. G.; Chan, F. T. *Phys. Rev. Lett.* **1991**, *67*, 2045.
(40) Larsson, S.; Volosov, A.; Rosén, A. *Chem. Phys. Lett.* **1987**, *137*, 501.
(41) Negri, F.; Orlandi, G.; Zerbetto, F. *Chem. Phys. Lett.* **1988**, *144*, 31.
(42) Kato, T.; Kodama, T.; Shida, T.; Nakagawa, T.; Matsui, Y.; Suzuki, S.; Shiromaru, H.; Yamauchi, K.; Achiba, Y. *Chem. Phys. Lett.* **1991**, *180*, 446.
(43) Kato, T.; Kodama, T.; Oyama, M.; Okazaki, S.; Shida, T.; Nakagawa, T.; Matsui, Y.; Suzuki, S.; Shiromaru, H.; Yamauchi, K.; Achiba, Y. *Chem. Phys. Lett.* **1991**, *186*, 36.
(44) Greaney, M. A.; Gorun, S. M. *J. Phys. Chem.* **1991**, *95*, 7142.
(45) Gasyna, Z.; Andrews, L.; Schatz, P. N. *J. Phys. Chem.* **1992**, *96*, 1525.
(46) Arbogast, J. W.; Foote, C. S.; Kao, M. *J. Am. Chem. Soc.* **1992**, *114*, 2277.
(47) Lawson, D. R.; Feldheim, D. L.; Foss, C. A.; Dorhout, P. K.; Elliot, C. M.; Martin, C. R.; Parkinson, B. *J. Electrochem. Soc.* **1992**, *139*, L68.
(48) Bertel, E.; Rosina, G.; Netzer, F. P. *Surf. Sci.* **1986**, *172*, L515.
(49) MacDonald, J. R.; Barlow, C. A., Jr. *J. Chem. Phys.* **1963**, *39*, 412; **1966**, *44*, 202.
(50) Heiney, P. A.; Fischer, J. E.; McGhie, A. R.; Romanow, W. J.; Denenstein, A. M.; McCauley, J. P., Jr.; Smith, A. B. III; Cox, D. E. *Phys. Rev. Lett.* **1991**, *66*, 2911.
(51) Mate, C. M.; Kao, C. T.; Somorjai, G. A. *Surv. Sci.* **1988**, *206*, 145.